Check for updates

# Synthesis, DNA interaction and SOD-like activities of copper(II) complexes: investigation of their DNA-interaction mechanism

Chun-Lian Zhang[1] · Dai-Hong Cai[1] · Shi Chen[1] · Wei Liu[2] · Ya-Hong Xiong[1] · Xue-Yi Le[1]

## Abstract

Two water-soluble 6-(pyrazin-2-yl)-1,3,5-triazine-2,4-diamine (pzta)-based Cu(II) complexes, [Cu(pzta)(L-LysH)(H$_2$O)] (ClO$_4$)$_2$·H$_2$O (**1**) and [Cu(pzta)(L-Phe)(H$_2$O)]ClO$_4$·0.75H$_2$O (**2**), (L-LysH = protonated L-lysinate; L-Phe = L-phenylalaninate), were synthesized and characterized. X-ray crystallography analysis revealed that the coordination geometries around Cu(II) in both complexes can be described as a distorted square pyramid, in which the pzta (N,N) and amino acids (N,O) both act as bidentate chelating ligands. The binding properties of the complexes toward calf thymus DNA (CT-DNA) were studied by physico-chemical and spectroscopic methods, together with viscosity measurements, and isothermal titration calorimetry. Overall, these studies indicated that both complexes associate with DNA via a groove binding mode, driven mainly by hydrophobic interactions. This conclusion is further supported by molecular docking calculations. In addition, the DNA cleavage and SOD-like activities of the complexes were investigated. We found that the complexes can cleave plasmid DNA efficiently in the presence of ascorbate through an oxidative pathway and they also have favorable SOD-like activities.

## Introduction

Copper(II) complexes have many important biological functions and also show promise as therapeutic reagents, DNA structural probes, DNA cleavage and footprinting agents, DNA condensing agents for gene delivery, and so on [1–3]. Recent studies have shown that some Cu(II) complexes of 1,3,5-triazine derivatives have anticancer, antibacterial and metalloenzyme activities, but the poor water solubility has tended to limit their biological applications [4, 5]. Meanwhile, the Cu(II) complexes with amino acid/dipeptide ligands often exhibit excellent solubility in water; hence, the water solubility of Cu(II)-1,3,5-triazine complexes may be improved by the use of amino acids as ancillary ligands [6–8]. Copper(II) complexes of aromatic heterocycles with amino acid co-ligands have gained a great deal of attention as potential models for metalloenzymes, such as superoxide dismutase (SOD) that can scavenge the toxic superoxide radical ($O_2^{-·}$) formed in all organisms, which may solve the problems of high cost and difficult in purification of natural SOD enzymes [9]. Furthermore, SOD enzyme mimics can affect tumor cell proliferation, due to the generation of increased amounts of H$_2$O$_2$ and hydroxyl radical (OH·), which are critically cytotoxic in affected cell lines [10, 11].

The interactions of metal complexes with DNA have received much attention owing to their biological applications and the development of novel therapeutic agents involving DNA binding and/or damaging properties [12–14]. A range of spectroscopic and physicochemical techniques can be used to study the interactions of metal complexes with DNA; however, isothermal titration calorimetry (ITC), although an effective technique for DNA-binding investigations, has been relatively underemployed [15–17].

In view of these observations, recently we have been interested in ternary Cu(II) complexes with 1,3,5-triazine derivatives and amino acid co-ligands [8, 18, 19]. In continuation of our interests in this area, here we report the synthesis and characterization of two Cu(II) complexes, formulated as [Cu(pzta)(L-LysH)(H$_2$O)](ClO$_4$)$_2$·H$_2$O (**1**) and [Cu(pzta)(L-Phe)(H$_2$O)]ClO$_4$·0.75H$_2$O, (**2**) (pzta = 6-(pyrazin-2-yl)-1,3,5-triazine-2,4-diamine; L-LysH = protonated

✉ Xue-Yi Le
lexyfu@163.com

1 Department of Applied Chemistry, South China Agricultural University, Guangzhou 510642, People's Republic of China

2 College of Materials and Energy, South China Agricultural University, Guangzhou 510642, People's Republic of China

L-lysinate; L-Phe:= L-phenylalaninate). The DNA binding and cleavage properties of the complexes were studied by multiple spectroscopic methods, viscosity measurements, ITC and agarose gel electrophoresis, as well as molecular docking methods, with special emphasis on their DNA-interaction mechanism being revealed. In addition, the $O_2^{.-}$ scavenging activities of the complexes were assayed using the modified nitroblue tetrazolium (NBT) photoreduction method.

## Experimental

### Materials

L-Lysine, L-phenylalanine, tris(hydroxymethyl)aminomethane (Tris), nitroblue tetrazolium (NBT) and Cu/Zn-SOD enzyme were obtained from Sinopharm Chemical Reagent Co., Ltd (China). Calf thymus DNA (CT-DNA), 3-[4,5-dimethylthiazol-2-yl]-2,5-diphenyl tetrazolium (MTT) and ethidium bromide (EB) were procured from Sigma. All other chemicals and solvents of analytical grade were purchased from commercial sources and used without further purification. Doubly distilled water was used as the solvent throughout the experiments.

CT-DNA and the complexes used for the DNA-binding experiments were prepared in Tris–HCl buffer (pH = 7.2) containing 5 mM Tris and 50 mM NaCl. The purity of DNA was checked by the UV absorbance ratio at 260/280 nm, which was in the range 1.8–1.9, indicating that the DNA was sufficiently free of protein. The concentration of DNA solution was determined through its absorption intensity at 260 nm with a molar extinction coefficient of 6600 $M^{-1}$ $cm^{-1}$ [20]. The stock solution of DNA was stored at 4 °C and was used within 4 days.

### Synthesis of [Cu(pzta)(L-LysH)(H$_2$O)](ClO$_4$)$_2$·H$_2$O (1)

A solution of Cu(ClO$_4$)$_2$·6H$_2$O (0.1850 g, 0.5 mmol) in water (0.5 mL) was added dropwise to a solution of pzta (0.0945 g, 0.5 mmol) in ethanol/water (20 mL, v/v: 3/1) with stirring, followed by addition of a solution of L-lysine (0.0731 g, 0.5 mmol) plus NaOH (0.0200 g, 0.5 mmol) in water (5 mL). The reaction mixture was stirred at 70 °C and then filtered. The resulting solution was allowed to slowly evaporate at room temperature, resulting in well-shaped crystals suitable for X-ray diffraction analysis. The product was collected, washed alternately with ethanol and water, and then dried in air. Yield: 78%. Anal. Calcd for C$_{13}$H$_{24}$Cl$_2$CuN$_9$O$_{12}$ (MW = 633.87) (%): C, 24.63; H, 3.98; N, 19.89. Found: C, 24.85; H, 4.23; N, 20.10. UV–visible $\lambda_{max}$/nm ($\varepsilon$/M$^{-1}$ cm$^{-1}$): $\pi - \pi^*$ 216 (27059), 278 (8913), d–d 630 (50). FTIR (KBr, cm$^{-1}$): $\nu$(OH), 3474w, $\nu_s$ (NH$_2$) 3331 m, $\nu_{as}$ (NH$_2$) 3157 m,

$\nu$(COO$^-$) 1654 s, 1381 m, $\nu$(C=N) 1590 s. Molar conductance, $\Lambda_M$ (1.0×10$^{-3}$ M, H$_2$O): 196.4 S$^{-1}$ cm$^2$ mol$^{-1}$.

### Synthesis of [Cu(pzta)(L-Phe)(H$_2$O)]ClO$_4$·0.75H$_2$O (2)

This complex was prepared by a procedure similar to that given above, but using L-phenylalanine (0.0826 g, 0.5 mmol) instead of L-lysine. Well-shaped blue plate crystals were obtained by slow evaporation of the reaction mixture. Yield: 83%. Anal. Calcd for C$_{16}$H$_{21.50}$ClCuN$_8$O$_{7.75}$ (MW = 548.90) (%): C, 35.01; H, 3.95; N, 20.41. Found: C, 35.33; H, 3.80; N, 20.60. UV–visible $\lambda_{max}$/nm ($\varepsilon$/M$^{-1}$ cm$^{-1}$): $\pi - \pi^*$ 217 (37346), 276 (10719), d–d 634 (82). FTIR (KBr, cm$^{-1}$): $\nu$(OH) 3404w, $\nu_s$(NH$_2$) 3350 m, $\nu_{as}$ (NH$_2$) 3169 m, $\nu$(COO$^-$) 1659 s, 1386 m, $\nu$(C=N) 1592 s. Molar conductance, $\Lambda_M$ (1.0×10$^{-3}$ M, H$_2$O): 98.7 S$^{-1}$ cm$^2$ mol$^{-1}$.

### X-ray crystallographic studies

Crystal data collections were performed on a Bruker Smart 1000 diffractometer equipped with a CCD area detector using Mo K$\alpha$ radiation ($\lambda$ = 0.071073 nm) with the $\varphi - \omega$ scan technique at 173 (2) K. The data were reduced by the SAINT program and corrected for absorption using the semiempirical multi-scan approach (SADABS). The structures were solved by direct methods and refined using the SHELX-2014 programs. Anisotropic thermal parameters of all non-hydrogens were refined by full-matrix least-squares based on |F|$^2$ using the SHELXTL program package. Their coordinates were determined by Fourier analyses with H atoms added theoretically and refined as riding atoms with fixed isotropic thermal parameters. Further crystallographic data and experimental details for both complexes are summarized in Table S1. Selected bond lengths (Å) and bond angles (°) are given in Table S2.

CCDC entries 924412 and 924410 for contain the supplementary crystallographic data for this paper. These data can be provided free of charge from The Cambridge Crystallographic Data Centre.

### DNA-binding experiments

Interactions of the complexes with CT-DNA were investigated on a Pharmacia 2550 UV–Vis spectrophotometer (Shimadzu, Japan) by varying the concentration of DNA from 0 to 17.13 μM while keeping the concentration of the test complex constant (55 μM). After addition of DNA to a solution of the complex, the mixture was kept for 5 min to equilibrate and the absorption spectra were then recorded in the range of 200–400 nm. The binding constants ($K_b$) were obtained from the spectroscopic titration data using the following equation [21]:

$$[DNA]/(e_a - e_f) = [DNA]/(e_b - e_f) + 1/K_b(e_b - e_f) \tag{1}$$

where [DNA] is the concentration of DNA, $\varepsilon_a$ is obtained by calculating $A_{obsd}$/[Cu] $\varepsilon_f$ and $\varepsilon_b$ correspond to the extinction coefficients of the unbound and fully bound compound, respectively. From the plots of [DNA]/$(\varepsilon_a - \varepsilon_f)$ versus [DNA], the binding constants $(K_b)$ were obtained from the ratio of the slope to the intercept.

Competitive binding assays between ethidium bromide and the complexes for CT-DNA were investigated with a Hitachi RF-4500 fluorescence spectrophotometer (Hitachi, Japan). The emission spectra of DNA solutions were recorded in the range of 540–660 nm with an excitation wavelength at 591 nm by adding the complexes (0–40 µM) to the EB-DNA system (EB: 4.8 µM, CT-DNA: 50 µM). The sample solutions were mixed and incubated at room temperature for 5 min before measurements. The quenching constants $(K_{sv})$ were calculated using the following Stern–Volmer equation [14]

$$I_0/I = 1 + K_{sv}[Q] \tag{2}$$

where $I_0$ and $I$ correspond to the fluorescence intensities of the EB-DNA system in the absence and presence of the complexes, respectively, and [Q] is the concentration of the complex.

Circular dichroism (CD) spectra of CT-DNA in the presence and absence of the complexes were recorded with a Chirascan CD spectropolarimeter (Applied Photophysics, UK) at room temperature while varying the [complex]/[CT-DNA] ratio ($r = 0.0, 0.2, 0.4$). Each sample solution was scanned in the range of 220–320 nm, and the final data were calculated by averaging three scans and subtracting the buffer background. These experiments were carried out under a nitrogen atmosphere.

Viscometric experiments were carried out with an Ubbelohde viscometer thermostated in a water bath maintained at $29.0 \pm 0.1$ °C, and the flow time was measured using a digital stopwatch. Each sample was measured three times, and the average flow time was calculated. The data were analyzed as $(\eta/\eta_0)^{1/3}$ versus $r$ ([complex]/[DNA] = 0, 0.05, 0.1, 0.15, 0.2, 0.25 and 0.3), where $\eta$ represents the viscosity of CT-DNA in the presence of the complex, and $\eta_0$ is the viscosity of the DNA alone. The viscosity values were calculated according to the relationship $\eta = (t - t_0)/t_0$, where $t$ and $t_0$ are the observed flow times in the presence and absence of the test samples, respectively [3]. A positive control experiment was performed under the same conditions but using EB instead of the complexes.

DNA melting experiments were carried out on a Chirascan CD spectropolarimeter (Applied Photophysics, UK) by monitoring the absorption at 260 nm of CT-DNA (500 µM) in the absence and presence of the complexes (200 µM). The temperature was increased from 40 to 99 °C at a rate of 3 °C/min, and the midpoint denaturation temperature $(T_m)$ of the CT-DNA solutions was recorded.

ITC experiments were performed using a VP-ITC isothermal titration calorimeter (Microcal Inc., Northampton MA, USA) at 25 °C. The complex (0.2 mM) was introduced into the syringe and the amount for each injection was 10 µL; then, CT-DNA (0.04 mM) was injected into the sample cell. The reference power was set as 10 µcal, and the stirring speed was adjusted to 307 rpm. All solutions used for ITC were degassed for a minimum of 5 min prior to the experiments, and a time interval of 120 s was set between two consecutive injections to allow for equilibration of the binding sites. ITC experiments gave a complete thermodynamic characterization profile of the DNA binding, specifically the enthalpy change ($\Delta H$), entropy change ($\Delta S$), stoichiometry ($n$) and binding constant ($K_b$). The data were analyzed according to the sequential binding mode of single binding sites using the Origin 7.0 software provided with the instrument. The change in free energy ($\Delta G$) was calculated according to the following formula [22]:

$$\Delta G = -RT \ln K_b = \Delta H - T\Delta S \tag{3}$$

where $T$ is the absolute temperature (298.15 K) and $R$ is the gas constant, 8.315 J mol$^{-1}$ K$^{-1}$.

The molecular docking studies of the complexes with DNA were performed using the Autodock 4.2 program. Calculations were carried out using a Lamarckian genetic algorithm (LGA). The X-ray crystal structures of the complexes were converted to the PDB format using Mercury software, and the crystal structure of the B-DNA dodecamer d(CGCGAATTCGCG)$_2$ (PDB ID: 1BNA) was taken from the Protein Data Bank. The water molecules were deleted, and the polar hydrogens of the macromolecule were added prior to docking calculations. The binding sites were defined by setting the grid size to $60 \times 60 \times 60$ Å with 0.375 Å grid space, and the complexes were centered at the coordinates $x = 14.779$, $y = 20.976$ and $z = 8.804$ at site of the DNA. The resulting complex–DNA model complexes were visualized using PyMol software.

## DNA cleavage experiments

The DNA cleavage activities of the complexes were assessed by agarose gel electrophoresis with a Powerpac Universal-JY200C instrument (Liuyi, Beijing) using supercoiled plasmid pEGM-3Zf (-) DNA. Samples containing DNA (200 ng), ascorbate (0.5 mM), Cu(ClO$_4$)$_2$·6H$_2$O (12.5 µM), pzta (12.5 µM), amino acids (12.5 µM) and Cu(II) complexes (variable concentration) in Tris–HCl buffer were incubated for 2 h at 37 °C, and then, the loading buffer (containing 0.25% bromophenol blue plus 0.25% xylene cyanol) (3 µL) was added. The final solutions (20 µL) were subjected to electrophoresis for 40 min at 100 V on 1% agarose gel containing SYBR Green $I$ (3 µL) in TAE buffer (40 mmol/L Tris acetate, 1 mmol/L EDTA, pH = 8.0). In

addition, the cleavage mechanisms of the complexes were investigated in the presence of typical radical scavengers, specifically hydroxyl radical scavengers (DMSO and methanol), and singlet-oxygen quenchers (2,2,6,6-tetramethyl-1-piperidinyloxy (TEMPO) and sodium azide). Each sample was tested according to the process described above. After electrophoresis, the bands were visualized under UV light and photographed using a Bio-Rad Laboratories-Segrate Gel Imaging System.

## Superoxide radical scavenging assays

The superoxide radical ($O_2^{-\cdot}$) scavenging activities of the complexes (0.05–0.8 μM) were assayed by a modified nitroblue tetrazolium (NBT) photoreduction method. A control experiment was carried out using the native SOD enzyme (Cu/Zn-SOD) in place of the complexes. A non-enzymatic system of TEMED-VB$_2$-NBT containing NBT (93.2 μM), riboflavin (6.80 μM) and tetramethyl-ethylenediamine (100 μM) in 0.05 M phosphate buffer at pH 7.8 was used. The redox reactions were monitored by detecting the absorbance of the reduced NBT (blue formazan) at 560 nm, and the inhibition ratios ($I$) of NBT reduction for the complexes were calculated according to the following equation [23]:

$$I(\%) = (1 - h/h_0) \times 100 \tag{4}$$

where $\eta_0$ and $\eta$ represent the slope of the straight line of absorbance values as a function of time in the absence and presence of the test compounds (complexes or native SOD enzyme), respectively. The 50% inhibition ($IC_{50}$) was obtained by plotting the percentage of inhibition versus concentration. The final $IC_{50}$ values were the average of triplicate experiments.

## Results and discussion

### Synthesis and characterization

The complexes were obtained by reacting copper(II) perchlorate with 6-(pyrazin-2-yl)-1,3,5-triazine-2,4-diamine and L-lysine or L-phenylalanine in a solvent mixture of ethanol and water. The resulting complexes were soluble in water and in Tris–HCl buffer (pH = 7.2). The elemental analyses (C, H and N) of both complexes confirmed their molecular formulae, and the molar conductance values in aqueous solution indicated that complex **1** is a 1:2 electrolyte, whereas complex **2** is a 1:1 electrolyte [24].

In the FTIR spectra, the presence of $\nu$(–OH) bands for both complexes indicated the presence of water in the crystal lattice. Bands in the range of 1700–1750 cm$^{-1}$ for the free amino acids were significantly shifted in the complexes,

suggesting coordination of the COO$^-$ groups to the central Cu(II) atom [24]. The magnitude of separation (> 200 cm$^{-1}$) between $\nu_{as}$(COO$^-$) and $\nu$(COO$^-$)$_s$ of the carboxylate in the spectra suggested monodentate coordination of these groups [25]. Additionally, $\nu$(C=N) of the coordinated pzta ligands was shifted to lower frequencies compared to free pzta (1636 cm$^{-1}$), indicating that the lone pair electrons on the amino nitrogen atom are involved in the formation of a coordinate bond with the metal bands at 640 and 480 cm$^{-1}$ in the spectra of the complexes that can be assigned to $\nu$(Cu–O) and $\nu$(Cu–N), respectively [26].

In the UV spectra of the complexes, the observed absorption bands be assigned to intra-ligand charge transfer transitions (π–π*) of pzta. Weak and broad bands in the visible regions arise from the d–d transition of the Cu(II) atom, suggesting a distorted square-pyramidal geometry [27].

The stabilities of the complexes in both aqueous and Tris–HCl buffer (pH = 7.2) solutions were measured by UV–Vis spectrophotometry over time intervals of 0, 12, 24 and 48 h at room temperature. The spectral profiles (Fig. S1 and S2†) revealed no dissociation of the complexes after 48-h incubation, suggesting that they are both sufficiently stable in water/Tris–HCl buffer solution for further studies [28].
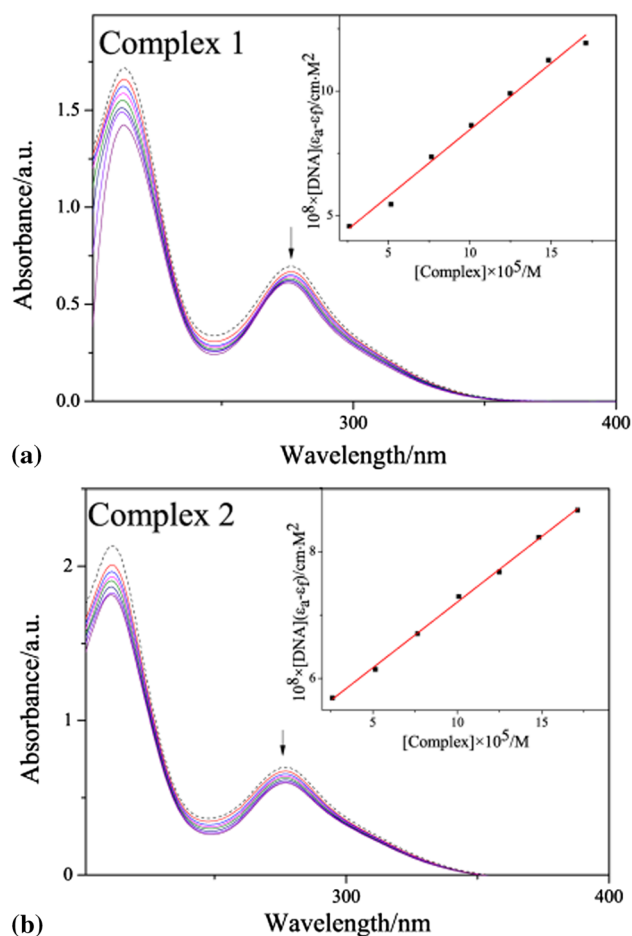
### X-ray crystal structures

The molecular structure of [Cu(pzta)(L-LysH)(H$_2$O)](ClO$_4$)$_2$ along with the atomic numbering scheme is shown in Fig. 1(a). This complex crystallizes in the triclinic space group P − 1. The central Cu(II) atom is five-coordinated with a slightly distorted square-pyramidal geometry as evident from the value of the geometric ($\tau$) parameter at 0.065 [$\tau = (\beta - \alpha)/60$, where $\alpha$ = N(8)–Cu(1)–N(1) = 171.6° (2), $\beta$ = O(1)–Cu(1)–N(7) = 175.5°(2)]. The basal plane is provided by two nitrogen atoms from the pzta ligand [Cu(1)–N(1) 2.021 (4) Å and Cu(1)–N(7) 2.020 (4) Å], together with the amino nitrogen atom and one carboxylate oxygen atom from L-LysH ligand [Cu(1)–N(8) 1.994 (4) Å and Cu(1)–O(1) 1.926 (4) Å]. The apical position is occupied by the water ligand [Cu(1)–O(1 W) 2.323 (5) Å]. The Cu–O(1 W) apical bond is much longer than the Cu–O(1) basal bond, which is a typical feature of the square-pyramidal configuration and agrees well with the geometry of the analogous square-pyramidal Cu(II) complex [Cu(nphen)(gly)(H$_2$O)]$_2$(NO$_3$)$_3$ (nphen = 5-nitro-1,10-phenanthroline) [26]. In addition, protonation (–NH$_3^+$) of the 5-amino group of L-lysinate leads to the formation of [Cu(pzta)(L-LysH)(H$_2$O)]$^{2+}$, which is similar to the previously reported complex [Cu(L-lysine)(2,2′-bipy)(H$_2$O)(ClO$_4$)$_2$] [25]. In the crystal structure, the mononuclear units of [Cu(pzta)(L-LysH)(H$_2$O)]$^{2+}$ are linked together by

**(a)**

**(b)**
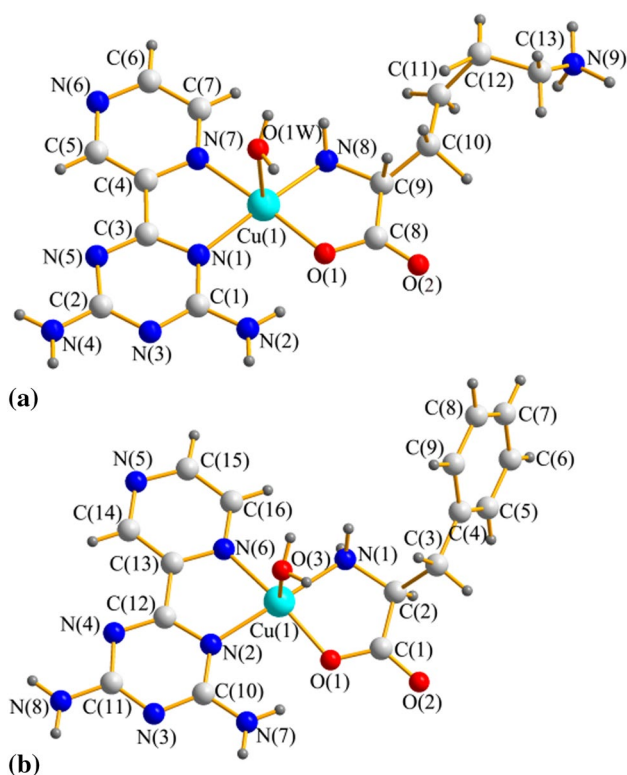
**Fig. 1** Structures of [Cu(L-LysH)(pzta)(H₂O)]²⁺ (**a**) and [Cu(L-Phe)(pzta)(H₂O)]⁺ (**b**). The perchlorate ions are omitted for clarity



**(a)**

**(b)**

**Fig. 2** Electronic absorption spectra of **1** (**a**) and **2** (**b**) in the absence and presence of CT-DNA. The arrows show the absorbance change upon increasing the DNA concentration. Inset: plots of $[DNA]/\varepsilon_a - \varepsilon_f$ versus [DNA]

intermolecular hydrogen-bond interactions [O2–H9CA⋯N9B (1.939Å); O2A–H9C⋯N9 (1.939 Å)].

The second complex, [Cu(pzta)(L-Phe)(H₂O)]ClO₄·0.75H₂O, has a structure consisting of complex cations [Cu(pzta)(L-Phe)(H₂O)]⁺, uncoordinated perchlorate anions (ClO₄⁻) and crystal waters. The complex cation unit (P2₁) is shown in Fig. 1(b). The bond distances around the metal center and donor sites are in the range of 1.925–2.251 Å, while the angles between the adjacent coordinate bonds fall in the range of 82.0(3)–99.0(3)°. The coordination geometry around Cu(II) is best described as a distorted square pyramid, as is evident from the value of the geometric ($\tau$) parameter, 0.18 [$\tau = (\beta - \alpha)/60$, where $\alpha = $ O(1)–Cu(1)–N(6) = 165.8° (2), $\beta = $ N(1)–Cu(1)–N(2) = 176.6° (2)]. The aromatic ring position of L-Phe is approximately perpendicular to the coordination plane formed by the CuN₃O atoms with an angle of 67.1°, which is similar to the previously reported complex [Cu(nphen)(L-tyr)(H₂O)]NO₃·2H₂O [27]. In the crystal structure, pairs of [Cu(pzta)(L-Phe)(H₂O)]⁺ cations are connected with each other by intermolecular hydrogen bonds between the non-coordinated carboxylate oxygen of L-Phe and one hydrogen of a water molecule [O2A–H3DA⋯O2 (1.897 Å)].

## DNA-binding experiments

### Electronic absorption titrations

Electronic absorption spectroscopy was employed to examine the binding mode between the complexes and DNA. In a typical case of intercalation, hypochromism and bathochromism of the spectral bands of metal complexes can be observed in the presence of DNA, but in the case of groove binding, in which the complex binds on the outer surface of DNA, little or no bathochromism is usually observed. As shown in Fig. 2, upon addition of increasing amounts of CT-DNA to the complexes, a decrease in the intensity (hypochromism) of the absorption peaks was observed, while the positions of the peaks were not changed, indicating that the interaction might be a groove binding mode, involving surface binding of the complexes to the DNA duplex via hydrogen bonds between the amino acid (–NH₂ and –COO⁻) and pzta (–NH₂) ligands and DNA. The

intrinsic binding constants ($K_b$) were obtained as $1.73 \times 10^4$ and $4.63 \times 10^3$ $M^{-1}$ for complex **1** and **2**, respectively, which are within the range of reported values ($10^3$–$10^5$ $M^{-1}$) for groove binders [29]. Furthermore, complex **1** showed a stronger DNA binding affinity than **2**. This may be attributed to the presence of the protonated amino group ($-NH_3^+$) in L-LysH, which might allow for additional hydrogen bonds with DNA.

## Ethidium bromide displacement assays

The binding between the complexes and CT-DNA was further studied by monitoring the emission intensity of DNA-bound ethidium bromide (EB) by fluorescence spectroscopy. Usually, EB emits intense fluorescence in the presence of CT-DNA, due to its strong intercalation between adjacent CT-DNA base pairs. However, addition of a second DNA-binding molecule can quench the fluorescence intensity of the EB-DNA system if the molecule can displace EB from the DNA-EB system [30]. The emission spectra of the EB-DNA system in the absence and presence of the complexes are illustrated in Fig. 3. Upon addition of the complexes to DNA-EB, the emission intensities decreased by 39.04% and 41.91% for **1** and **2**, respectively, indicating that the complexes can compete with EB for DNA due to intercalation or groove binding. According to the classical Stern–Volmer equation, the obtained quenching constant ($K_{sv}$) values were $4.047 \times 10^4$ $M^{-1}$ for complex **1** and $3.451 \times 10^4$ $M^{-1}$ for complex **2**, with the order of **1 > 2**, consistent with the results obtained by electronic absorption spectroscopy.

## Circular dichroism spectroscopy

Circular dichroism (CD) spectroscopy is a useful technique for the detection of changes in DNA morphology during complex–DNA interactions. Generally, the CD spectra of CT-DNA show little or no perturbation for electrostatic or groove binding, but significant changes for intercalation modes [31]. As shown in Fig. 4, two major bands observed at 275 (positive) and 245 nm (negative) correspond to the base stacking and the B-type DNA, respectively. On addition of the complexes to CT-DNA, both the negative and positive bands were slightly shifted toward longer wavelengths, suggesting that the secondary structure of the CT-DNA double helix has been translated from the B to C conformation [32]. These changes support our hypothesis that these complexes interact with DNA in a groove binding mode, in agreement with the results described above.
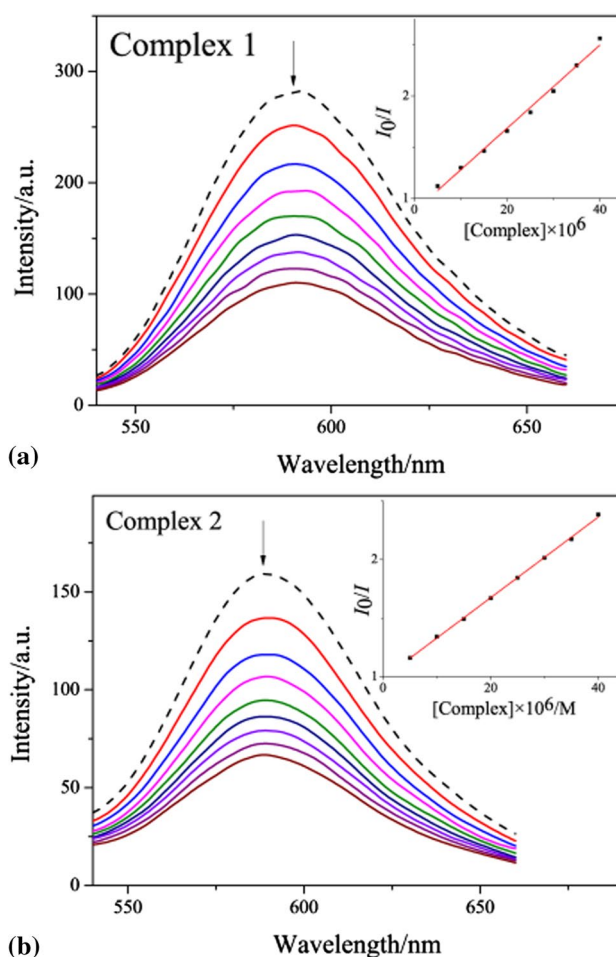


**Fig. 3** Emission spectra of the EB-CT-DNA system in the absence and presence of **1** (**a**) and **2** (**b**). Inset: plots of $I_0/I$ versus [Complex]. Arrows show the changes in intensity with increasing concentration of CT-DNA

## Viscosity measurements

Viscosity measurements are sensitive to change in the length of DNA and are regarded as one of the most important methods to clarify the binding mode of DNA in solution. A classical intercalative mode causes a significant increase in DNA viscosity due to increasing DNA length, whereas partial or non-intercalative binding modes such as electrostatic interactions may produce a bend in the DNA helix, causing a decrease in viscosity, and the groove binding mode typically results in little or no effect on DNA viscosity [16]. The effects of the present complexes on the viscosities of CT-DNA are shown in Fig. 5. Evidently, with increasing concentrations of the complexes, the relative viscosity of CT-DNA was marginally changed compared with the viscosity of EB-CT-DNA system. These
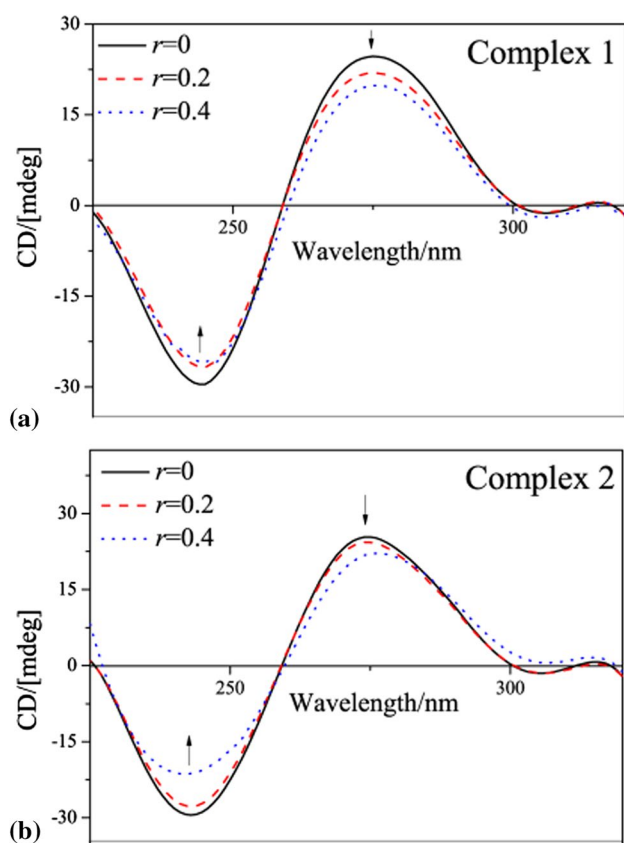
**Fig. 4** CD spectra of CT-DNA in the absence and presence of **1** (**a**) and **2** (**b**) at room temperature. Conditions: [DNA] = $1.0 \times 10^{-4}$ M, $r$ = [Complex]/[DNA] = 0, 0.2, 0.4
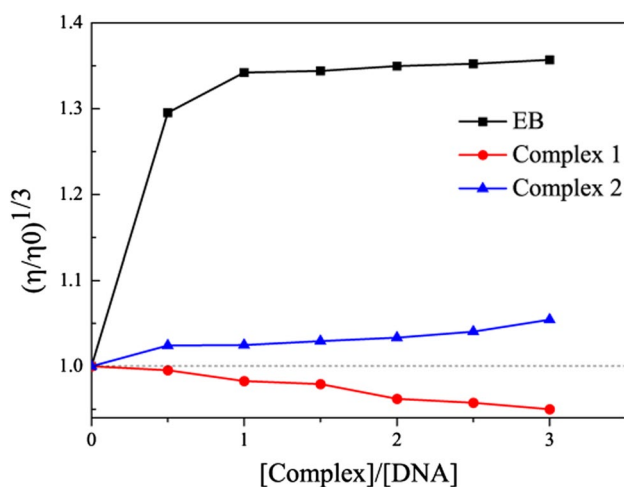


**Fig. 5** Relative viscosities of CT-DNA upon addition of increasing amounts of **1** (a), **2** (b) or EB. Conditions: [DNA] = 0.2 mM, [Complex]/[DNA]: = 0, 0.05, 0.10, 0.15, 0.20, 0.25, 0.30

results further confirm that the complexes associate with DNA in a groove binding mode, in agreement with the spectroscopic results.

## Thermal denaturation experiments

Thermal denaturation analysis is an important method for the elucidation of DNA-binding modes of metal complexes. In general, a considerable increase in the melting temperature (5–8 °C) is expected for intercalative binding of the complex to DNA, while no obvious increase in melting temperature is observed in the case of groove and/or electrostatic binding modes [34]. In this work, DNA melting experiments were carried out by monitoring the absorption (260 nm) of CT-DNA at various temperatures in the absence and presence of the complexes. The melting temperature curves of CT-DNA under these conditions are shown in Fig. 6. The melting temperature ($T_m$) of CT-DNA alone was 86.62 °C, and those of the DNA–complex systems were 88.36 and 88.08 °C for **1** and **2**, respectively. These minor shifts in melting temperature indicate that the complexes bind to DNA via a non-intercalative binding mode, which is again concordant with the results discussed above.

## Isothermal titration calorimetry assays

Isothermal titration calorimetry (ITC) experiments were performed to get further insight into the binding and thermodynamic parameters for the interaction between the complexes and DNA [17]. The ITC profiles are shown in Fig. 7, in which the upper panels show the representative raw ITC profiles as a result of the injection of the complexes into CT-DNA, while the lower panels show the heats of reaction plotted against the molar ratio of the complexes to CT-DNA after correcting the baseline. The ITC profile clearly shows that the binding of the complexes to the DNA is endothermic and fits well with a single site binding model. The binding constants, thermodynamic parameters and stoichiometries
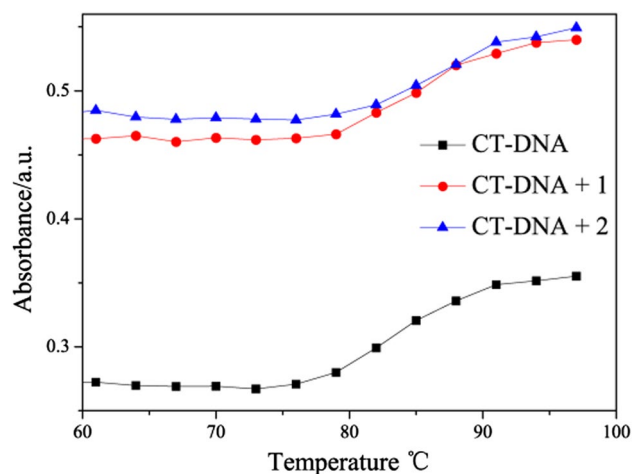


**Fig. 6** Thermal melting profiles of CT-DNA in the absence and presence of **1** (a) and **2** (b) at 260 nm

**Fig. 7** ITC data for the titration of **1** (**a**) and **2** (**b**) into CT-DNA solution at 25 °C. The top panels represent the heat burst curves for successive injection of the complexes into the DNA. The bottom panels represent the corresponding normalized heat signals versus molar ratio fitted to one-site model
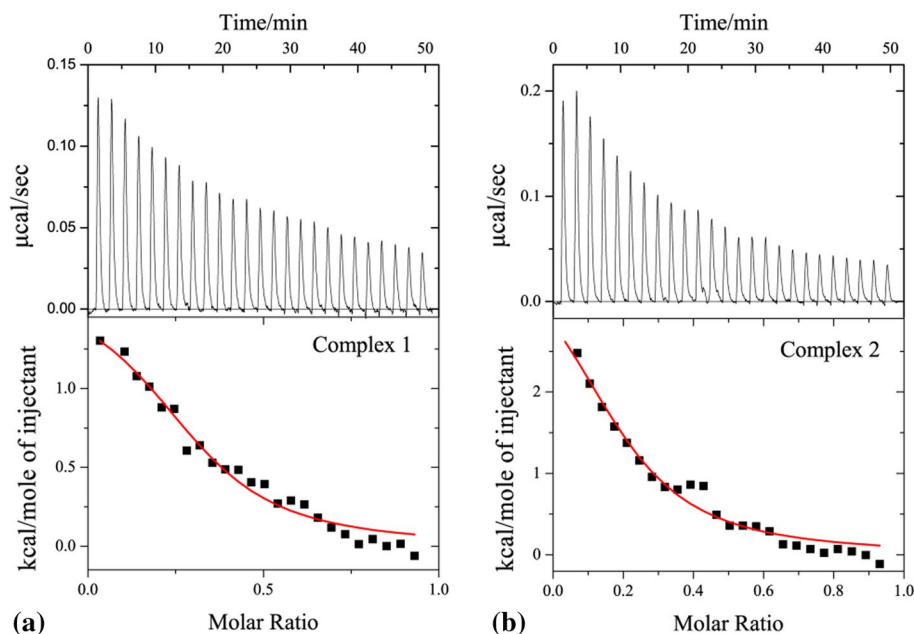


**Table 1** The thermodynamic parameters obtained by the ITC experiments for the CT-DNA binding of the complexes

| Complex | $n$ | $K_b \times 10^5$ (L mol$^{-1}$) | $\Delta H$ (kcal/mol) | $-T\Delta S$ (kcal/mol) | $\Delta G$ (kcal/mol) |
|---|---|---|---|---|---|
| **1** | $0.313 \pm 0.0207$ | $3.22 \pm 0.756$ | $1.516 \pm 0.152$ | $-9.183$ | $-7.667$ |
| **2** | $0.206 \pm 0.0312$ | $2.45 \pm 0.657$ | $4.085 \pm 0.793$ | $-11.449$ | $-7.364$ |

are summarized in Table 1. The negative values of $\Delta G$ confirm that the complexes bind to DNA in a spontaneous processes, and the positive values of $\Delta H$ and $\Delta S$ indicate that hydrophobic forces dominate the binding process, although a contribution from hydrogen bonds and van der Waals forces cannot be ruled out. Based on our results, it can be reasonably inferred that H-bond interactions may be responsible for the binding affinities ($K_b$) of the complexes to CT-DNA following the order **2 > 1**.
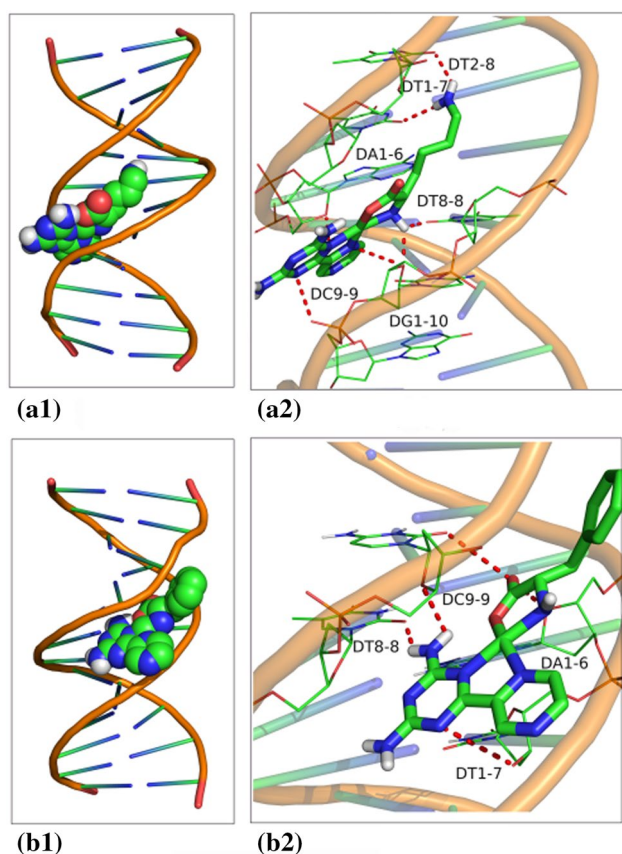
## Molecular docking analyses

Molecular docking simulation is a useful tool for investigating the potential binding modes and energies in complex–DNA systems [35]. We have modeled the interaction of these complexes with DNA (PDB entry 1BNA) to confirm the results obtained from the experimental studies. The most energetically favorable conformations of the docked structures of the complexes with DNA are illustrated in Fig. 8. The resulting docked models show that the complexes are situated in the minor groove of DNA within the region of GC–TA consecutive base pairs through van der Waals forces, hydrophobic and hydrogen-bond interactions. The calculated binding energies for the docked Cu(II) complexes with DNA were −12.45 and −9.73 kcal·mol$^{-1}$ for [Cu(pzta)(L-LysH)(H$_2$O)](ClO$_4$)$_2$·H$_2$O and [Cu(pzta)(L-Phe)(H$_2$O)]

ClO$_4$·0.75H$_2$O, respectively, indicating a stronger DNA binding affinity of the former compared with the latter. This can be attributed to the binding of [Cu(pzta)(L-LysH)(H$_2$O)](ClO$_4$)$_2$·H$_2$O to DNA via three hydrogen bonds, namely complex: H8A…1BNA:DC99: O4 (2.159 Å), complex: H9A…1BNA:DT28: O2 (2.128 Å) and complex: H9B…1BNA:DT17: O2 (2.210 Å). In contrast, only one hydrogen bond (complex: H15…1BNA:DT88: O2 (1.917 Å) was observed for the [Cu(pzta)(L-Phe)(H$_2$O)]ClO$_4$·0.75H$_2$O-DNA complex. The results obtained from the molecular docking simulation correlated well with the experimental findings.
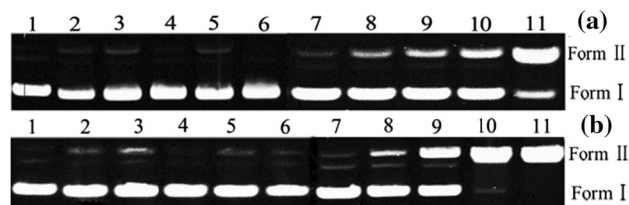
## Chemical nuclease activities

To explore the DNA cleavage abilities of the complexes, supercoiled (SC) pEGM-3Zf(-) DNA was incubated with each complex and the cleavage reactions were assayed by agarose gel electrophoresis. When circular plasmid DNA is subjected to electrophoresis, the fastest migration will be observed for the supercoiled form (Form I). If one DNA strand is cleaved, the supercoiled form will be relaxed to produce a slower-moving nicked circular form (Form II). Once both strands of the DNA are cleaved, a linear form (Form III) will be produced, with a migration rate between those of forms I and II [35]. As shown in
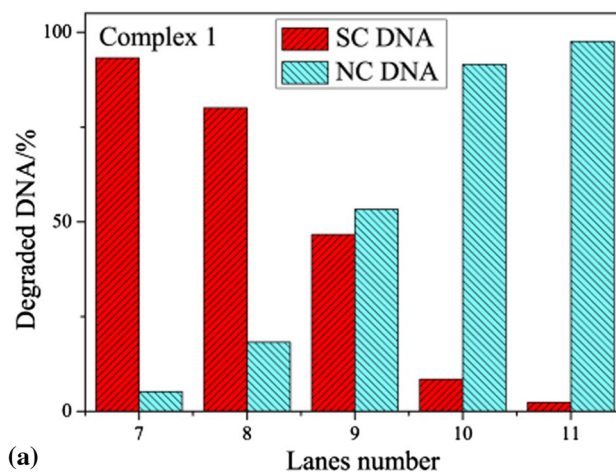
**Fig. 8** The molecular docked poses of **1** (**a**) and **2** (**b**) with DNA (1-BNA). (1) The perspectives of the complexes binding to DNA; (2) detailed views of the docking poses of the DNA–complex systems
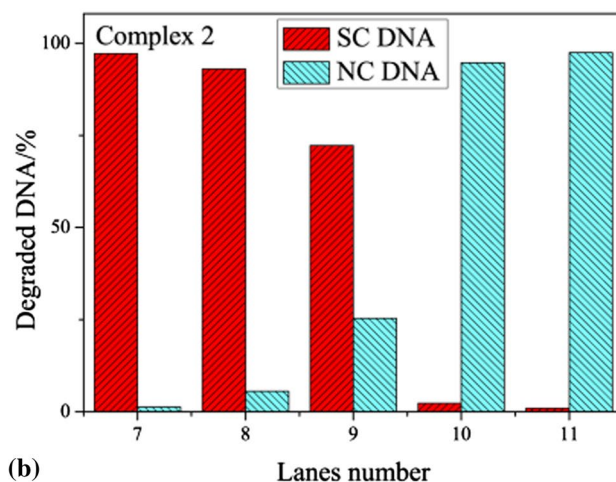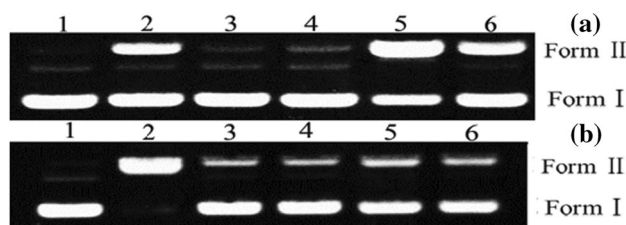


**Fig. 10** The relative amounts of different DNA forms obtained after incubation with **1** (**a**) and **2** (**b**) (lanes 7–11), respectively



**Fig. 9** Cleavage of plasmid DNA (200 ng) by **1** (**a**) and **2** (**b**). Lane 1, DNA control; lane 2, DNA + ascorbate (0.625 mM); lane 3, DNA + ascorbate (0.625 mM) + Cu(ClO$_4$)$_2$·6H$_2$O (12.5 µM); lane 4, DNA + ascorbate (0.625 mM) + pzta (12.5 µM); lane 5, DNA + ascorbate (0.625 mM) + L-Lys/L-Phe (12.5 µM); lane 6, DNA + complex (12.5 µM); lanes 7–11, DNA + ascorbate (0.625 mM) + complex **1** (10, 15, 20, 25 and 30 µM)/complex **2** (4, 6, 8, 10 and 12 µM)



**Fig. 11** Cleavage of plasmid DNA (200 ng) by **1** (**a**) (15 µM) and **2** (**b**) (8 µM) in the presence of various reactive oxygen species scavengers. Lane 1, DNA control; lane 2, DNA + ascorbate (0.625 mM) + complex; lane 3, DNA + ascorbate (0.625 mM) + complex + DMSO (200 µM); lane 4, DNA + ascorbate (0.625 mM) + complex + methanol (200 µM); lane 5, DNA + ascorbate (0.625 mM) + complex + TEMPO (200 µM); lane 6, DNA + ascorbate (0.625 mM) + complex + NaN$_3$ (200 µM)

Fig. 9, the control experiments showed that ascorbate, Cu(ClO$_4$)$_2$, pzta or L-Lys/L-Phe (lanes 2–6) exhibited no obvious DNA cleavage, but both complexes could efficiently cleave DNA in a concentration-dependent manner in the presence of ascorbate (lanes 7–11). Compared with [Cu(pzta)(L-LysH)(H$_2$O)](ClO$_4$)$_2$·H$_2$O, [Cu(pzta)(L-Phe)

(H$_2$O)]ClO$_4$·0.75H$_2$O exhibited stronger DNA cleavage activity (Fig. 10), which may be related to its higher DNA binding affinity.
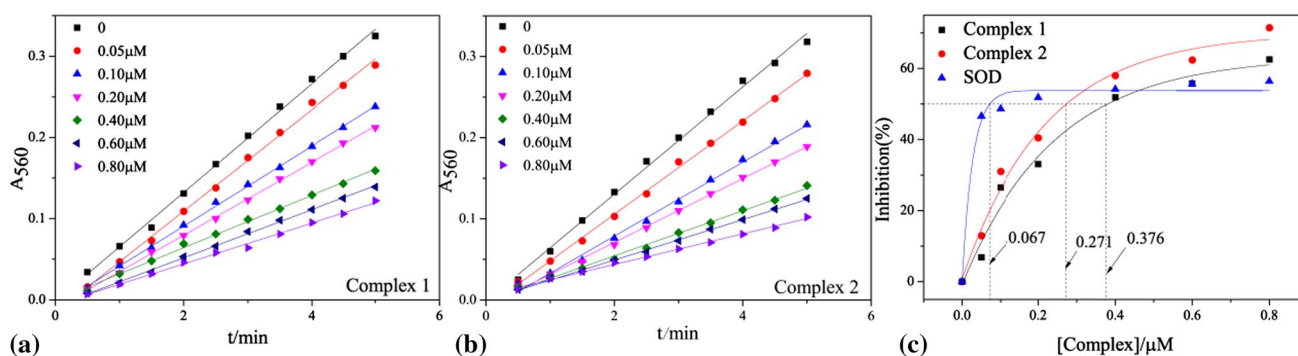
**Fig. 12** Plots of inhibition of **1** (**a**) and **2** (**b**) against superoxide anion radical versus the concentration of the complex

In order to characterize the DNA cleavage mechanism of the complexes, several typical scavengers were used in further experiments (Fig. 11). Evidently, the DNA cleavage activities of the complexes were inhibited significantly in the presence of hydroxyl radical scavengers (DMSO and methanol) (lanes 3 and 4), suggesting that ·OH plays an important role in the cleavage process. On the other hand, singlet-oxygen scavengers (TEMPO and NaN$_3$) could clearly inhibit the cleavage activity of [Cu(pzta)(L-Phe)(H$_2$O)]ClO$_4$·0.75H$_2$O, indicating that $^1O_2$ is involved in the cleavage reaction for the complex. Hence, the DNA cleavage mechanisms of the two complexes appear to be somewhat different.

## SOD-like activities

Superoxide dismutase is the main enzyme responsible for the catalytic the dismutation of superoxide anion (O$_2^{\cdot-}$) radical to hydrogen peroxide and molecular oxygen, providing an important defense against oxidative damage to DNA and proteins within the human body [10]. As shown in Fig. 12, the average inhibition ratios of the complexes against superoxide anion radical increased with their concentrations. The SOD-like activities of the complexes and the native SOD enzyme are presented as IC$_{50}$ values, expressing the concentration required for 50% inhibition of NBT reduction. Both complexes exhibited excellent SOD-like activities, with IC$_{50}$ values of 0.376 and 0.271 μM for [Cu(pzta)(L-LysH)(H$_2$O)](ClO$_4$)$_2$·H$_2$O and [Cu(pzta)(L-Phe)(H$_2$O)]ClO$_4$·0.75H$_2$O, respectively. Although their activities were weaker than those of the native Cu–Zn-SOD (IC$_{50}$ = 0.067 μM), the complexes can still be considered as potent SOD mimics in view of their lower molecular weights compared to the enzyme. The scavenging O$_2^{\cdot-}$ mechanism for the complexes might involve a direct attack of O$_2^{\cdot-}$ at the free axial position of the five-coordinate Cu(II) to give a six-coordinated adduct, which should be quite unstable due to the Jahn–Teller effect. Rapid reduction of Cu(II) to Cu(I) would then follow with the release of an oxygen molecule. The Cu(I) center can be re-oxidized into the Cu(II) by a further molecule of O$_2^{\cdot-}$, with

concomitant production of hydrogen peroxide, as reported for similar Cu(II) complexes [11].

## Conclusions

In this research, two new Cu(II) complexes of pzta with amino acid co-ligands were synthesized and characterized. Both complexes have distorted square-pyramid geometries with N3O2 coordination environment. In vitro DNA-binding experiments revealed that the complexes associate with DNA via a groove binding mode, mainly driven by hydrophobic forces. The complexes are capable of efficiently inducing double-strand plasmid DNA breaks via an oxidative pathway involving the formation of hydroxyl and/or singlet-oxygen free radicals in the presence of ascorbate. In addition, both complexes exhibit high superoxide dismutase-like activities. These results will inspire us to design new DNA structural probes, DNA cleavage and footprinting agents and new therapeutic reagents for diseases.

## References

1. Deo KL, Pages BJ, Ang DL, Gordon CP, Aldrich-Wright JR (2016) Int J Mol Sci 17:1818–1835
2. Santini C, Pellei M, Gandin V, Porchia M, Tisato F, Marzano C (2013) Chem Rev 114:815–862
3. Mohanraj M, Ayyannan G, Raja G, Jayabalakrishnan C (2016) Mater Sci Eng, C 69:1297–1306
4. Qi YY, Gan Q, Liu YJ, Xiong YH, Mao ZW, Le XY (2018) Eur J Med Chem 154:220–232
5. Chen JW, Wang XY, Shao Y, Zhu JH, Zhu YG, Li YZ, Xu Q, Guo ZJ (2007) Inorg Chem 46:3306–3312
6. Micskei K, Patonay T, Caglioti L, Palyi G (2010) Chem Biodivers 7:1660–1669
7. Kirin SI, Dubon P, Weyhermüller T, Bill E, Metzler-Nolte N (2005) Inorg Chem 44:5405–5415

8. Zhang CL, Zhang XM, Liu W, Chen S, Mao ZW, Le XY (2017) Appl Organomet Chem 32:e3994
9. Daier VA, Rivière E, Mallet-Ladeira S, Moreno DM, Hureau C, Signorella SR (2016) J Inorg Biochem 163:162–175
10. Siddiqi ZA, Sharma PK, Shahid M, Khalid M (2012) Anjuli, Siddique A, Kumar S. Eur J Med Chem 57:102–111
11. Gan Q, Zhang CL, Wang BF, Xiong YH, Fu YL, Mao ZW, Le XY (2016) Rsc Adv 6:35952–35965
12. Chitrapriya N, Shin JH, Hwang IH, Kim Y, Kim C, Kim SK (2015) Rsc Adv 5:68067–68075
13. Bruijnincx PCA, Sadler PJ (2008) Curr Opin Chem Biol 12:197–206
14. Zhao XF, Ouyang Y, Liu YZ, Su QJ, Tian H, Xie CZ, Xu JY (2014) New J Chem 38:955–965
15. Erxleben A (2018) Coord Chem Rev 360:92–121
16. Haris P, Mary V, Haridas M, Sudarsanakumar C (2015) J Chem Inf Model 55:2644–2656
17. Turnbull WB, Daranas AH (2003) J Am Chem Soc 125:14859–14866
18. Zhang XM, Ou ZB, Chen S, Xiong YH, Zhou XH, Liu HF, Le XY (2012) Chin J Inorg Chem 28:2667–2673
19. Shen F, Ou ZB, Liu YJ, Liu W, Wang BF, Mao ZW, Le XY (2017) Inorg Chim Acta 465:1–13
20. Bera R, Sahoo BK, Ghosh KS, Dasgupta S (2008) Int J Biol Macromol 42:14–21
21. Jana K, Maity T, Mahapatra TS, Das Mohapatra PK, Debnath SC, Das S, Hossain M, Samanta BC (2017) Transit Metal Chem 42:69–78
22. Ahmad I, Ahmad M (2015) Int J Biol Macromol 79:193–200
23. Andrasi M, Lehoczki G, Nagy Z, Gyemant G, Pungor A, Gaspar A (2015) Electrophoresis 36:1274–1281
24. Pal A, Chaudhary S (2013) Thermochim Acta 573:200–205
25. Thebo KH, Shad HA, Thebo AA, Raftery J (2014) J Crystallogr Rep 59:1063–1067
26. İnci D, Aydın R, Vatan O, Sevgi D, Yılmaz D, Zorlu Y, Yerli Y, Çoşut B, Demirkan E, Çinkılıç N (2017) J Biol Inorg Chem 22:61–85
27. Inci D, Aydın R, Vatan O, Yılmaz D, Genckal HM, Zorlu Y, Cavas T (2015) Spectrochim Acta A 145:313–324
28. Lian WJ, Wang XT, Xie CZ, Tian H, Song XQ, Pan HT, Qiao X, Xu JY (2016) Dalton Trans 45:9073–9087
29. Draksharapu A, Boersma AJ, Leising M, Meetsma A, Browne WR, Roelfes G (2015) Dalton Trans 44:3647–3655
30. Sundaravadivel E, Kandaswamy M, Varghese B (2013) Polyhedron 61:33–44
31. Arjmand F, Muddassir M, Yousuf I (2014) J Photoch Photobio B 136:62–71
32. Haribabu J, Jeyalakshmi K, Arun Y, Bhuvanesh NSP, Perumal PT, Karvembu R (2015) Rsc Adv 5:46031–46049
33. Rehman SU, Sarwar T, Husain MA, Ishqi HM, Tabish M (2015) Arch Biochem Biophys 576:49–60
34. Holt PA, Chaires JB, Trent JO (2008) J Chem Inf Model 48:1602–1615
35. Loganathan R, Ramakrishnan S, Ganeshpandian M, Bhuvanesh NSP, Palaniandavar M, Riyasdeen A, Akbarsha MA (2015) Dalton Trans 44:10210–10227